15.8 LARGE-EDDY SIMULATIONS OF THERMALLY INDUCED OSCILLATIONS IN THE CONVECTIVE BOUNDARY LAYER

Marcus Oliver Letzel *† and **Siegfried Raasch**
Institute of Meteorology and Climatology, University of Hannover, Hannover, Germany

1. INTRODUCTION

Inhomogeneity on a wide range of spatial and temporal scales is a key feature of the Earth's surface. Variability in, for example, terrain, vegetation, soil texture and wetness, and land-use leaves its first imprints on the atmosphere in the atmospheric boundary layer (ABL). The sudden or gradual changes in radiative, thermal, moisture and aerodynamic surface properties such as surface heat, momentum and humidity fluxes, surface roughness, temperature, wetness, and elevation affect the ABL flow structure and associated atmospheric processes, e.g. alter convection.

The heterogeneous surface information usually translates into the ABL dynamically or thermally. Both have been subject of active research over the past two decades (e.g., Pielke 2001). Recent Large-eddy simulation (LES) case studies (e.g., Avissar and Schmidt 1998; Gopalakrishnan and Avissar 2000; Baidya Roy and Avissar 2000) point at heterogeneous surface heat fluxes playing a key role here. Via differential ABL heating they produce horizontal pressure gradients that initiate a mesoscale circulation. The effect of such a thermally induced mesoscale circulation (TMC) can extend well into the free atmosphere up to the mid-troposphere (Dalu et al. 2000).

This numerical study reveals for the first time that in many cases the TMC onset induces a temporal oscillation of ABL flow, which significantly changes average statistical properties and mean profiles. It shows how the oscillation depends on the inhomogeneity scale, provides a hypothesis of the oscillation mechanism and briefly discusses TMC power spectra.

Surface heat flux heterogeneity is idealized as simple sine waves in order to bring out the new oscillation phenomenon most clearly. Simulations of complex heterogeneous conditions are in preparation.

2. NUMERICAL EXPERIMENT

This study used the *PA*rallelized *L*ES *M*odel PALM developed by Raasch and Schröter (2001) – see also paper P3.13 in this preprint volume. Detailed model description is available on-line from Raasch (2002).

The starting point of this research was an open question of the study by Avissar and Schmidt (1998; hereafter AS98), hence the experimental design follows their case study to allow comparison.

2 h after simulation start, one-dimensional sinusoidal variations of amplitude A_x on wavelengths λ_x from 2.5 to 40 km were imposed on the near surface potential temperature flux $\overline{w'\theta'}$ (hereafter simply referred to as surface heat flux) so that

$$\overline{w'\theta'}(x) = \overline{w'\theta'}_{av} + A_x \sin\left(\frac{2\pi}{\lambda_x} x\right) \quad .$$

Large-scale subsidence was applied to the potential temperature profile only (Khairoutdinov and Kogan 1999), but in contrast to AS98 a much weaker, more realistic subsidence velocity of -2 cm s^{-1} was used. The Coriolis effect was disabled for simplicity.

All simulations were run with a uniform grid spacing of 50 m, with 9% vertical stretching above 1,800 m. The domain size was 5 km in *y*- and 3.2 km in *z*-direction. The width D_x was generally chosen large enough to juxtapose at least two waves within the model domain, to allow potential eddy interaction over more than one wavelength and to clearly resolve the spectral signals. D_x is listed along with other simulation parameters for cases with zero background wind in Table 1.

Cases with light wind have been discussed by Letzel and Raasch (2002), available on-line from Raasch (2002), along with further additional material. For cases with larger wind see paper P6.18 in this preprint volume.

Calculations were carried out until at least two or three oscillation peaks were obtained. The cases denoted with a lower case "h" are corresponding homogeneous control runs. Case A15 was run to reproduce the results of AS98 and is labeled accordingly.

The atmosphere was initialized with a weakly stable profile ($\partial\theta/\partial z$ = 0.8 K km^{-1}) up to a height of 1,200 m and a strong capping inversion above ($\partial\theta/\partial z$ = 7.4 K km^{-1}).

TABLE 1 (t_s: simulation time; other parameters cf. text)

Case	D_x	λ_x	$\overline{w'\theta'}_{av}$	A_x	t_s
	km	km	K m s^{-1}	K m s^{-1}	h
A15	40	40	0.24	0.20	12
A15h	40	–	0.24	0	12
L1	10	2.5	0.16	0.15	6
L1h	10	–	0.16	0	6
L2	10	5.0	0.16	0.15	6
L3	15	7.5	0.16	0.15	6
L4	20	10	0.16	0.15	9
L4h	20	–	0.16	0	11
L5	30	15	0.16	0.15	9
L6	40	20	0.16	0.15	9
L7	50	25	0.16	0.15	9
L7h	50	–	0.16	0	9
L8	30	30	0.16	0.15	11

* *Corresponding author address:* Marcus Letzel, Institut für Meteorologie und Klimatologie, Universität Hannover, Herrenhäuser Str. 2, 30419 Hannover, Germany; letzel@muk.uni-hannover.de
† On leave at: Department of Civil Engineering, Tokyo Institute of Technology, Tokyo, Japan

FIGURE 1 Vertical heat flux profiles of cases A15 and A15h at selected times, averaged horizontally and over the last 15 minutes. The contribution of parameterized sub-gridscale (SGS) heat flux (dashed-dotted lines) is almost negligible.

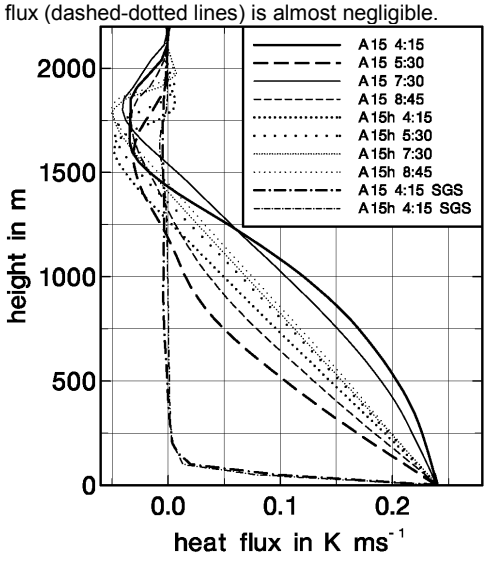

FIGURE 2 Time series of kinetic perturbation energy E* for cases L1 to L8 with homogeneous control cases L4h and L7h. Cases L1 to L8 have same heat flux mean and amplitude but differ in wavelength and simulation time. For explanation of IDE* see section 3.2.

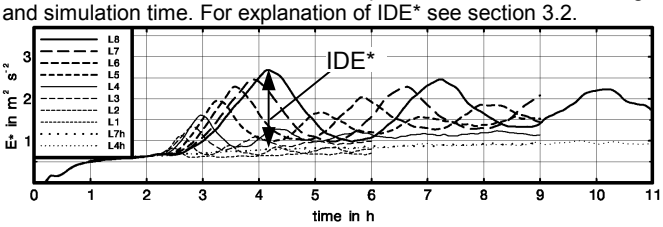

FIGURE 3 2D *x-t* time series of *p* in Pa (contour) and *u* in m s^{-1} (grayscale) for case L4. Decription see text.

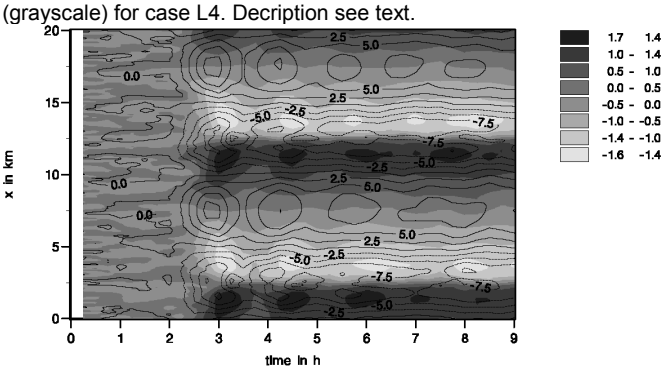

3. RESULTS

TMCs have already been well investigated (cf. section 1). PALM reproduces the results of AS98 well (Letzel and Raasch 2002). The results focus on the thermally induced oscillation.

Vertical profiles, time series, and power spectra were used for ABL flow analysis.

3.1. *The Oscillation – Fundamentals*

3.1.a) OSCILLATION EXISTENCE

One of the main findings of this study is that the TMC intensity itself varies with time. AS98 already observed nonlinear vertical heat flux profiles at 4h30 (esp. for their case A15), which clearly points at non-quasi steady CBL development, but they could not observe oscillations because their simulations lasted only 4.5h.

In the present study, as soon as the heat wave is activated at 2 h, the linear vertical heat flux profile of case A15 turns convex and reaches its maximum curvature at 4h15. Then it slowly changes to a near linear shape and turns concave with a maximum curvature at 5h30, returns to convex (7h30) and again concave shape (8h45). Fig. 1 shows the profiles with extreme curvature together with the corresponding linear profiles of the homogeneous control run A15h.

In other words, at times, the upper part of the CBL is heated more strongly than the lower one (convex shape), and vice versa (concave). And indeed, the vertical profiles of potential temperature (Fig. O-1; Figures preceded by "O-" are available only on-line from Raasch 2002) exhibit a sequence of stabilization followed by destabilization that corresponds well to the observed temporal variation of the heat flux profiles.

Strong evidence of the oscillation is provided by time series of domain-averaged kinetic perturbation energy E* for cases L1 to L8 in Fig. 2 that describe a sine-like oscillation after the heat wave activation. The oscillation amplitude A_o, however, decreases with time, presumably due to friction near the ground and in the entrainment layer (momentum exchange with non-moving air aloft). (Fig. 1 shows that the maximum curvature, too, decreases with time.) Note that also the mean energy level itself increases dramatically compared with the homogeneous control runs.

3.1.b) OSCILLATION MECHANISM – A HYPOTHESIS

The point about the oscillation mechanism is not so much the TMC onset itself (attributable to horizontal surface heat flux, temperature and pressure gradients) – the key question seems to be what causes the TMC intensity to *decrease* (and *then* increase) again (Fig.2).

Fig. 3 shows 2D *x-t* time series of perturbation pressure *p* and *u* for case L4 that have been obtained in a three-step process: a) *xz* cross-sections of *p* and *u* (averaged in *y*-direction and over 15 minutes) are computed all throughout the simulation, b) these cross-sections are evaluated at height $z = 0.05\ z_i$ (z_i = ABL height), and c) they are then plotted as *x* vs. *t* time series overlay of *p* (contour) and *u* (grayscale). When the heat wave is activated at *t* = 2h, not only the temperature gradient (not shown), but also the pressure gradient immediately starts to build up. The TMC – as represented by *u* (and *w*, not shown) – follows with a phase lag of some 15 minutes. As the TMC grows in strength, the pressure gradient reaches its maximum and then begins to weaken. The TMC peak strength coincides with a rapid decrease of the pressure gradient. This cycle repeats itself in fairly regular intervals

with decreasing peak strength, which indicates that p and u oscillate around some equilibrium state.

Fig. 3 suggests that the TMC itself effectively reduces the horizontal pressure and temperature gradients that were responsible for its onset. Both gradients being reduced, the TMC itself also decreases in strength. Meanwhile, the surface heat wave of course continues, thus acting to restore the gradients. This explains why the TMC intensity then again rises to the next peak.

Note that – except for the oscillation – the pressure and velocity pattern basically remain the same until the end of the simulation and clearly reflect the forcing heat wave compared with the homogeneous pattern before t = 2h.

3.2. *The Oscillation – Parameter Space*

This section shows how the oscillation (A_o, T_o) depends on the perturbation wavelength λ_x. Oscillation dependence on background wind and perturbation amplitude is discussed by Letzel and Raasch (2002).

The time series of E* for cases L1 to L8 (Fig. 2) differ in both oscillation period T_o and amplitude A_o. The larger λ_x, the larger T_o and A_o.

However, the smallest wavelengths, λ_x = 2.5 and 5 km (L1, L2), do not produce clear oscillations, and their average energy level even drops below that of the homogeneous control cases (L4h, L7h).

Fig. 2 further suggests that though the initially clear oscillations of cases L3 to L8 may cease after some time, their energy level will probably still remain much higher than in the homogeneous control cases.

Fig. 4a shows that T_o depends almost linearly on λ_x. As the oscillation amplitude A_o is difficult to measure i) because of its decrease with time and ii) because of the slowly rising mean energy level, Fig. 4b instead depicts the initial departure IDE* of kinetic energy E* from its corresponding homogeneous value. (Fig. 2 shows how to derive IDE*.) However, IDE* has no clear linear relationship with λ_x.

T_o depends on the speed of the TMC onset. A large perturbation wavelength λ_x (weak horizontal surface heat flux gradient) or a small perturbation amplitude A_x (weak inhomogeneous heating) impede a quick TMC onset: the horizontal pressure gradients necessary for the TMC onset take longer to build up and reach the threshold.

IDE* increases with the perturbation wavelength λ_x. This is a nonlinear effect, because the TMC forcing, the horizontal surface heat flux gradient *d*ecreases with wavelength. The energy cascade may serve to explain this. At wavelengths near its peak at the natural scale of convection (2-3 km), the horizontal gradients due to the imposed inhomogeneities compete with those generated by the largest CBL eddies in natural convection and have to overcome their inertia to set up a TMC on this scale. At large wavelengths, however, this problem may not be so severe because on these scales the natural turbulence intensity has decreased by about an order of magnitude, making TMC generation easier.

Souza et al. (2000) presented a theory based on the second law of thermodynamics (the surface heat flux is proportional to the vertical temperature gradient at ground level) that explains why surface inhomogeneities enhance the CBL circulation (hence increase the kinetic energy level). Under homogeneous conditions, the surface heat flux decreases when an air parcel advects towards an updraft because as it heats up, the difference between its own and the ground surface temperature decreases. However, in case of horizontal surface temperature gradients, the surface heat flux then decreases less rapidly. This allows higher horizontal temperature and pressure gradients.

This study, however, directly prescribed the surface heat fluxes. Thus, while the air parcel approaches the updraft, in the inhomogeneous case the surface heat flux even increases further (as prescribed), whereas in the homogeneous case it remains constant. Therefore, directly prescribed inhomogeneous surface heat fluxes also lead to a speed-up compared with prescribed homogeneous surface heat fluxes.

FIGURE 4 Dependence of a) oscillation period T_o and b) initial departure IDE* of kinetic energy E* from homogeneous control case on the perturbation wavelength λ_x. Linear trend lines are added. Error bars indicate the variability of T_o in the individual time series. For derivation of IDE* see Fig. 2.

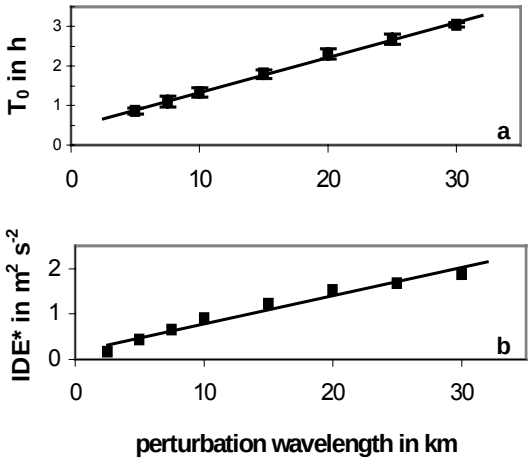

3.3. *TMC Spectral Characteristics*

The increased average kinetic energy level (Fig. 2) is only the integral result of the TMC effect on CBL turbulence. This section investigates how the TMC changes the spectral properties of CBL turbulence.

The last three hours of case L4 (when the oscillations are fading down but the domain average kinetic perturbation energy E* remains high) and its homogeneous control case L4h serve as a representative example for all cases. From power spectra computed in x- and y- direction of velocity components u, v, and w, Fig. 5 displays only those panels with a spectral TMC signal, namely the x-power spectra of u and w.

Shape and magnitude of the homogeneous turbulence spectra (L4h) agree well with previous findings (Kaimal et al. 1976). The inhomogeneous turbulence spectra (L4) show a main spectral peak at the wave

FIGURE 5 *x*-power spectra of velocity components a) *u* and b) *w*, time-averaged over *t* = 6-9h, calculated at z_i-normalized heights for cases L4 and L4h:

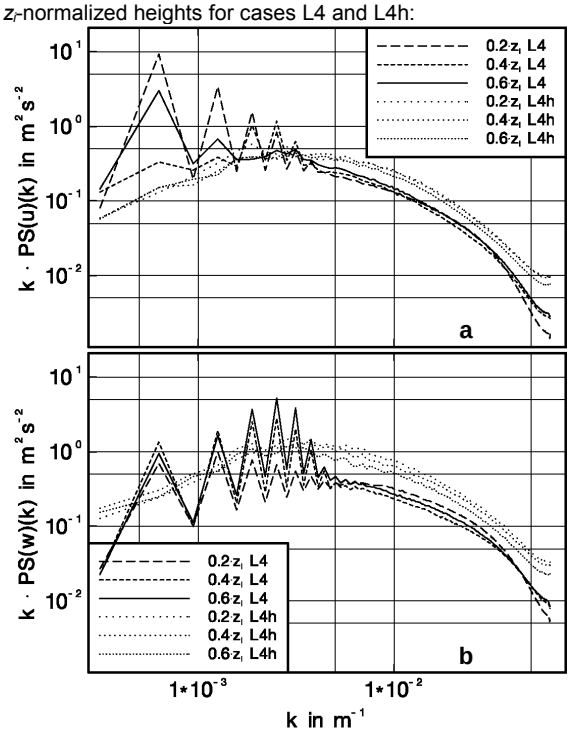

number k_x of the forcing surface heat wavelength λ_x ($k_x = 2\,\pi / \lambda_x = 6.3 \cdot 10^{-4}$ m^{-1}) plus a number of harmonics, spectral peaks at integral fractions of λ_x that account for the asymmetric open-cell ABL convection (Fig. 5).

Neither the *y*-power spectra nor the *x*-power spectrum of *v* reveal such TMC signals (Fig. O-2). This is because the model has been set-up homogeneously in *y*-direction. To the contrary, here, and also at the small scales in *x*-direction (Fig. 5), the turbulence intensity is suppressed, due to the large-scale subsidence caused by the TMC.

4. SUMMARY AND CONCLUSIONS

This study showed that the onset of TMCs on scales of 5km and more triggers off oscillations whose period and amplitude depend on the thermal surface forcing scale and intensity. With the TMC onset, the kinetic energy level increases markedly and remains significantly higher than in the homogeneous case.

Power spectra, however, show enhanced TMC signals only for the variables, directions and scales directly affected; otherwise turbulence is suppressed.

These new findings might call into question those turbulence parameterizations employed by general circulation and other large-scale models that rely entirely on homogeneous control runs of high-resolution models. The domain averaged value of the sinusoidal surface heat flux used in this study exactly equals that of a homogeneous model run, but kinetic energy, for instance, on which many sub-gridscale parameterizations are based, and spectra deviate considerably.

The highly idealized character of this study and its predecessors calls for further research using more realistic surface conditions, for example diurnal or 2D heat flux variations, a superposition of inhomogeneities of different wavelength, amplitude, dimension and form, and the like.

Experimental proof is likely to be impeded by the high degree of complexity of natural landscapes and spatial as well as temporal heat flux variations. Nevertheless, we expect an atmospheric response on the scale of strongest surface inhomogeneity. TMC oscillations may occur e.g. over Antarctic coastal polynyas, over continental lakes or patches of differently watered agricultural monocultures during summer. The upcoming EVA-GRIPS experiment in Germany is expected to give first answers to such questions.

Acknowledgements: This research was supported by the Studienstiftung des deutschen Volkes in Bonn, Germany, and German BMBF Grants 07ATF37-UH and 01LD0103. Most calculations were performed on the SGI/CRAY-T3E of the Konrad-Zuse-Zentrum für Informationstechnik (ZIB) in Berlin, Germany. The authors wish to thank M. Kanda, R. Moriwaki (Tokyo Inst. of Technology, Japan), Y. Noh (Yonsei Univ., Korea), D. Etling, T. Hauf and M. Herold (Univ. of Hannover, Germany) for their valuable comments and suggestions.

REFERENCES

Avissar, R., and T. Schmidt, 1998: An evaluation of the scale at which ground-surface heat flux patchiness affects the convective boundary layer using large-eddy simulation. *J. Atmos. Sci.,* **55**, 2666–2689.

Baidya Roy, S., and R. Avissar, 2000: Scales of response of the convective boundary layer to land-surface heterogeneity. *Geophys. Res. Lett.,* **27**, 533–536.

Dalu, G.A., R.A. Pielke, P.L. Vidale, and M. Baldi, 2000: Heat transport and weakening of atmospheric stability induced by mesoscale flows. *J. Geophys. Res.,* **105**, 9349–9363.

Gopalakrishnan, S.G., and R. Avissar, 2000: An LES study of the impacts of land surface heterogeneity on dispersion in the convective boundary layer. *J. Atmos. Sci.,* **57**, 352–371.

Kaimal, J.C., J.C. Wyngaard, D.A. Haugen, O.R. Coté, Y. Izumi, S.J. Caughey, and C.J. Readings, 1976: Turbulence structure in the convective boundary layer. *J. Atmos. Sci.*, **33**, 2152–2169.

Khairoutdinov, M.F., and Y.L. Kogan, 1999: A large eddy simulation model with explicit microphysics: Valication against aircraft observations of a stratocumulus-topped boundary layer. *J. Atmos. Sci.,* **56**, 2115–2131.

Letzel, M.O., and S. Raasch, 2002: Large-Eddy Simulation of Thermally Induced Oscillations in the Convective Boundary Layer. *Annual. J. Hydraulic Eng., JSCE*, **46,** 67-72

Pielke, R.A., 2001: Influence of the spatial distribution of vegetation and sooils on the prediction of cumulus convective rainfall. *Rev. Geophys.,* **39**, 151–177.

Raasch, S., cited 2002: PALM research group. [Available on-line from http://www.muk.uni-hannover.de/~raasch/PALM_group.]

—, and M. Schröter, 2001: PALM – A large-eddy simulation model performing on massively parallel computers. *Meteorol. Z.,* **10**, 363–372.

Souza, E.P., N.O. Renno, and M.A. Silva Dias, 2000: Convective circulations induced by surface heterogeneities. *J. Atmos. Sci.,* **57**, 2915–2922.